J Therm Anal Calorim (2012) 107:573–584
DOI 10.1007/s10973-011-1457-1

Synthesis and characterization of new complexes of some divalent transition metals with 2-acetyl-pyridyl-isonicotinoylhydrazone

Lucica Viorica Ababei · Angela Kriza · Cristian Andronescu · Adina Magdalena Musuc

Received: 31 January 2011 / Accepted: 7 March 2011 / Published online: 18 March 2011

Abstract Ten new mononuclear complexes having general formulae $[ML_2](ClO_4)_2$, M = Cu(II), Co(II), Ni(II), Mn(II) and Zn(II), $[ML_2](SO_4)$, M = Co(II), Ni(II) and $[ML_2(H_2O)_2](SO_4)$, M = Cu(II), Mn(II) and Zn(II), L = 2-acetyl-pyridyl-isonicotinoylhydrazone have been synthesized and characterized based on elemental analyses, IR spectroscopy, UV–Vis–NIR, EPR, as well as thermal analysis and determination of molar conductivity and magnetic moments. The structures of $[CoL_2](ClO_4)_2$ are accomplished by single crystal X-ray diffraction. The coordination sphere is formed by two N, N, O tridentates 2-acetyl-pyridyl-isonicotinoylhydrazone ligands, or by two N, O bidentate 2-acetyl-pyridyl-isonicotinoylhydrazone and two water molecules. Biological activity studies reveal a moderate activity of complexes against gram-negative and gram-positive bacteria.

Keywords 2-Acetyl-pyridyl-isonicotinoylhydrazone · Antimicrobial activity · Crystal structure · Schiff base · Thermal analysis · Transition metal complexes

L. V. Ababei (✉)
The House of Teaching Staff Giurgiu, 8, Nicholae Droc Barcian Street, Giurgiu, Romania
e-mail: lucica_32@yahoo.com

A. Kriza
Faculty of Chemistry, University of Bucharest, 23 Dumbrava Rosie Street, Bucharest, Romania

C. Andronescu · A. M. Musuc
"Ilie Murgulescu" Institute of Physical Chemistry, Romanian Academy, 202 Independence Avenue, 060021 Bucharest, Romania

Introduction

Schiff bases play an important role in inorganic chemistry as they easily form stable complexes with most transition metal ions. The development of the field of bioinorganic chemistry has increased the interest in Schiff base complexes, since it has been recognized that many of these complexes may serve as models for biologically important species [1–3].

The remarkable biological activity of acid hydrazides R–CO–NH–NH_2, a class of Schiff bases, their corresponding aroylhydrazones, R–CO–NH–N=CH–R and the dependence of their mode of chelating with transition metal ions present in the living systems have been of significant interest [4, 5]. The coordination compounds of aroylhydrazones have been reported to act as enzyme inhibitors and are useful due to their pharmacological applications [6, 7]. Isonicotinic acid hydrazide (INH) is a drug of proven therapeutic importance and is used as bacterial ailments, e.g. tuberculosis [8]. Hydrazones derived from condensation of isonicotinic acid hydrazide with pyridine aldehydes have been found to show better antitubercular activity than INH [9]. The coordination chemistry of Schiff base ligands derived from 2-pyridyl ketones has received more and more attention. In 1990, Gourbatsis and co-workers found a rich and varied coordination chemistry of Schiff base ligands derived from 2-acetylpyridine and 2-benzoylpyridine [10]. Particularly, tridentate ONO/S, NNO/S and PNO/S functionalized ligands have recently attracted considerable interest [11, 12], but surprisingly NNO-chelating ligands have been little published [13–15]. The tautomerism of these ligands as well as the well known transition metal chelating properties allows various structural possibilities [16] for its metal complexes. In the context of our previous research, a number of complexes of transition

metals with 2-acetylpyridine, 2-pyridyl-ketones or isonicotinoylhydrazone were obtained and characterized [17–19].

In the present paper, it was reported the synthesis and characterization of ten combinations of Cu(II), Co(II), Ni(II), Mn(II) and Zn(II) perchlorate and sulphate, with 2-acetyl-pyridyl-isonicotinoylhydrazone (L). The structural formula of ligand is shown in Fig. 1.

Experimental

Materials

All chemicals were of pure analytical grade and were purchased from Sigma-Aldrich and Fluka.

Synthesis of 2-acetyl-pyridyl-isonicotinoylhydrazone

The 2-acetyl-pyridyl-isonicotinoylhydrazone was obtained by refluxing on water bath for 5 h, a mixture of isoniazid (0.2742 g, 0.002 mol) and 2-acetyl-pyridine (0.1214 g, 0.002 mol) (ratio 1:1 molar). Methanol (30 mL) was used as a solvent. After cooling, a white precipitate occurs. This was filtered, washed with methanol and dried in vacuum on $CaCl_2$.

Synthesis of complexes

A methanolic solution of isoniazid (0.2742 g, 0.002 mol in 30 mL of methanol) is added to the methanolic solution of 2-acetyl-pyridine (0.1214 g, 0.002 mol in 30 mL methanol). The mixture was stirred at 50 °C for 30 min, cooled at room temperature and this was added under stirring, to the methanolic solution of Cu(II), Co(II), Ni(II), Mn(II) and Zn(II) perchlorate or sulphate (0.001 mol in 15 mL methanol). After 24 h, the complexes are precipitates. The solid products were filtered, washed with methanol and dried in vacuum over anhydrous $CaCl_2$. The $[CoL_2](ClO_4)_2$ complex was separated from single crystals and the X-ray crystal structure has been made.

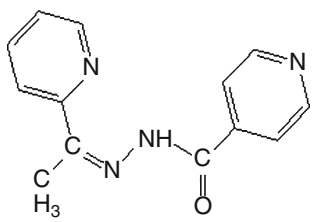

Fig. 1 The structural formula of 2-acetyl-pyridyl-izonicotinoylhydrazone (L)

Methods and apparatus

The elemental analyses (C, H, N) were made with an Elemental Combustion System CHNS-O, using a Costech device, type ECS 4010. The metal (II) contents were determined by gravimetric methods: Cu with salicylaldoxime, Ni with dimethilglioxime, and Co, Mn and Zn as pyrophosphates.

The melting temperatures of the complexes were directly measured with SMPI Melting Point Apparatus (Stuart Scientific). The molar conductance of the complexes was measured in 10^{-3} M DMF at room temperature using a Consort type C-533 conductivity instrument.

The IR spectra (4000–400 cm^{-1}) were recorded in KBr pellets, using a BIO-RAD FTS-135 spectrometer. The UV–Vis–NIR electronic spectra (200–2200 nm) were recorded with a UV–Vis–NIR spectrophotometer in diffuse reflectance on a JASCO V 670 spectrophotometer.

The measurements of magnetic susceptibility were determined at room temperature, using the Faraday method, and electronic paramagnetic resonance (EPR) spectra of Cu(II) complexes were recorded at room temperature, on a Jeol JESS FA 100 spectrometer, with a 100 Hz field modulation.

The thermal experiments were performed on a Mettler Toledo TGA/SDTA 851^e thermal analyzer, within the temperature range 300–1300 K. The TG curves were recorded in nitrogen atmosphere with a flow rate of 50 mL min^{-1} and at a heating rate of 10 K min^{-1}. The samples were held in alumina crucibles. Sample mass was between 0.8 and 1.5 mg. The TG/DTA curves were used to characterize the accompanying mass and heat changes during the linear heating.

Single-crystal X-ray diffraction was used for crystal structure determination of $[CoL_2](ClO_4)_2$ complex. XRD data were collected on a STOE IPDS II diffractometer operating with a Mo Kα radiation ($\lambda = 0.71073$ Å) and with a X-ray tube with a graphite monochromator, at room temperature. Data were collected using Stoe X-AREA [20] and cell refinement was made using Stoe X-AREA [20]. The structures were solved by direct methods and refined with anisotropic displacement parameters based on F^2, using SHELXS-97 and SHELXL-97 crystallographic software packages [21].

Antibacterial studies

The antibacterial activity of the ligand and its complexes was evaluated by the well diffusion technique [22] (Kirby Bayer method), in a medium of agar nutrient and using ciprofloxacin, gentamycin and ampicillin as control.

Table 1 Analytical and physical data of the complexes

Compounds	Colour	Melting point/°C	Λ^a/Ω^{-1} cm^2 mol^{-1}	$\mu_{eff}/_{BM}$	Elemental analysis Found (Calcd.)			
					M%	C%	H%	N%
$[CuL_2](ClO_4)_2$ (I)	Dark green	312[c]	135	1.72	8.253	38.612	3.464	15.224
					(8.556)	(38.775)	(3.257)	(15.079)
$[CoL_2](ClO_4)_2$ (II)	Brown	289[b]	176	4.33	7.512	36.309	3.310	14.199
					(7.393)	(36.133)	(3.035)	(14.051)
$[NiL_2](ClO_4)_2$ (III)	Brown	237[b]	177	3.20	7.045	36.358	3.286	14.289
					(7.365)	(36.144)	(3.036)	(14.056)
$[MnL_2](ClO_4)_2$ (IV)	Yellow	295	154	6.01	6.698	36.047	3.321	14.354
					(6.927)	(36.314)	(3.050)	(14.122)
$[ZnL_2](ClO_4)_2$ (V)	Yellow	288	175	dia	8.298	35.532	3.302	13.722
					(8.138)	(35.842)	(3.01)	(13.938)
$[CuL_2(H_2O)_2](SO_4)\cdot 2.5H_2O$ (VI)	Green	216	–	1.866	8.679	42.992	4.547	15.604
					(8.817)	(43.288)	(4.615)	(15.539)
$[CoL_2](SO_4)\cdot H_2O$ (VII)	Pink	>325	–	4.852	9.144	47.49	4.203	17.236
					(9.022)	(47.77)	(4.012)	(17.148)
$[NiL_2](SO_4)\cdot 3H_2O$ (VIII)	Blue	>325	–	2.80	8.745	45.472	4.154	16.496
					(8.519)	(45.290)	(4.389)	(16.258)
$[MnL_2(H_2O)_2](SO_4)\cdot 1.5H_2O$ (IX)	Yellowish	>325	–	5.654	7.722	44.786	4.598	16.376
					(7.914)	(44.948)	(4.501)	(16.135)
$[ZnL_2(H_2O)_2](SO_4)\cdot 3H_2O$ (X)	White	>325	–	dia	8.885	42.458	4.411	15.592
					(8.938)	(42.647)	(4.684)	(15.309)

[a] DMF solution 10^{-3} M at 20 °C, [b] With carbonization, [c] With explosion

Preparation of discs

The samples (1 mg ligand, respectively, complex compound in 1 mL DMF) were applied with a micropipette on paper discs of 3 mm diameter. The discs were left in an incubator for 48 h at 37 °C and then different species of bacteria grown on blood agar plates were applied on.

Culture media

- Blood agar medium (from bioMerieux) was used for the growth of specific gram-positive bacterial species: *Staphylococcus aureus.*
- CLED agar medium (from bioMerieux) was used for the growth of specific gram negative bacterial species: *Escherichia coli.*
- Mueller–Hinton 2 agar + 2% sheep blood medium (from bioMerieux) was used for the application of the paper discs in the case of *Salmonella Typhimurium.*

Application

Sterilized forceps were used for the application of the paper discs on the Mueller–Hinton plates. When the discs were applied, they were incubated at 37 °C for 24 h. The zone of inhibition around the disc was then measured (in mm).

Results and discussion

The complexes were characterized based on elemental analysis, magnetic susceptibility and electronic conductibility measurements, IR, UV–Vis, EPR and thermal studies. The complexes were coloured powders with high melting points. The perchlorate complexes are soluble in DMF, methanol, ethanol and acetone and insoluble in diethyl ether and chloroform. The molar conductivity values in DMF show that they are 1:2 type electrolytes [23]. The sulphate complexes are insoluble in common organic solvents (methanol, ethanol, acetone, diethyl ether, chloroform, DMF).

The analytical data show that the complexes may be formulated as $[ML_2](ClO_4)_2$, M = Cu(II), Co(II), Ni(II), Mn(II) and Zn(II), $[ML_2](SO_4)$, M = Co(II), Ni(II), and $[ML_2(H_2O)_2](SO_4)$, M = Cu(II), Mn(II) and Zn(II), L = 2-acetyl-pyridyl-isonicotinoylhydrazone.

The analytical and physical properties (colour, melting point and molar conductivity in DMF 10^{-3} M) of the complexes are given in Table 1.

Crystal structure description

The crystallographic data for the $[CoL_2](ClO_4)_2$ complex are summarized in Table 2. Selected bond lengths and angles are given in Table 3.

Crystallographic analysis reveals that the complex $[CoL_2](ClO_4)_2$ belongs to space group $P21/n$. Each molecular unit is composed by complex divalent cations $[Co(INHMPC)_2]^{+2}$ with two perchlorate groups as counter anions. Each Co(II) centre is in a distorted octahedral geometry having six coordinating environment by two azomethine nitrogen (Co–N7 = 1.848(5), Co–N3 = 1.845(4) Å), two pyridine nitrogen (Co–N8 = 1.921(4), Co–N4 = 1.925(4) Å) and two carbonylic oxygen (Co–O1 = 1.904(3), Co–O2 = 1.913(3) Å) from the two 2-acetyl-pyridyl-isonicotinoylhydrazone ligands (Fig. 2).

Formally, the complex units define the zigzag rows which are arranged in parallel according to the sequence ABAB, where the discrimination factor is the opposite direction of the chelated tridentates ligands (Fig. 3). Thus, layers with profiles of "zipper" are generated. The layers are placed parallel and they are separated by wave planes containing ClO_4^- anions and solvent molecules.

Mononuclear complexes form supramolecular chains parallel to each other via π-π type interactions stacking. Within such a supramolecular chain, two adjacent complex units have opposite orientations (Fig. 4).

It is noted that methanol molecule participates in hydrogen bonding. In the formation of hydrogen bonds are involved either O10A atom (O11···O10A = 2.461(2) Å) or atom O9 (O11···O9 = 3.058(2) Å), both belonging to the type of anion ClO_4^- (Fig. 5).

Table 2 Crystal data for the complex $[CoL_2](ClO_4)_2$

Chemical formula	$C_{27}H_{24}Cl_2CoN_8O_{11}$
M/g mol^{-1}	766.37
Temperature/K	293(2)
Wavelength/Å	0.71073
Crystal system	Monoclinic
Space group	$P21/n$
a/Å	11.2526(6)
b/Å	13.3767(9)
c/Å	20.7681(11)
α/^{0}	90.00
β/^{0}	95.751(4)
γ/°	90.00
V/Å^3	3110.3(3)
Z	4
F(000)	1564
Reflections collected	5606
Unique reflections	4107
R factor	0.0697
Goodness-of-fit on F^2	1.024

x, y, z; $-x + 1/2, y + 1/2, -z + 1/2$; $-x, -y, -z$; $x - 1/2, -y - 1/2, z - 1/2$

Infrared spectra

The main bands from IR spectra of ligand and its metal complexes are presented in Table 4.

In the 2-acetyl-pyridyl-isonicotinoylhydrazone IR spectra, a very intensive band appears at 1670 cm^{-1} and a strong band appears at 1623 cm^{-1}, which are assigned to the vibration frequency ν(C=O) amide I [24] and ν(C=N)

Table 3 Selected bond lengths (Å) and bond angles (°) for the complex $[CoL_2](ClO_4)_2$

$C_{27}H_{24}Cl_2CoN_8O_{11}$	
Bond angles (°)	
N3–Co1–N4	82.9(2)
N3–Co1–N7	177.8(2)
N3–Co1–N8	97.2(2)
N3–Co1–O1	82.3(2)
N3–Co1–O2	97.8(2)
N4–Co1–N7	99.3(2)
N4–Co1–N8	92.0(2)
N4–Co1–O1	165.1(2)
N4–Co1–O2	90.8(2)
N7–Co1–N8	83.1(2)
N7–Co1–O1	95.5(2)
N7–Co1–O2	81.9(2)
N8–Co1–O1	91.2(2)
N8–Co1–O2	165.0(2)
O1–Co1–O2	89.8(1)
Bond lengths (Å)	
N3–Co1	1.845(4)
N4–Co1	1.925(4)
N7–Co1	1.848(5)
N8–Co1	1.921(4)
O1–Co1	1.904(3)
O2–Co1	1.913(3)
O3–Cl1	1.549(11)
O4–Cl1	1.429(6)
O5–Cl1	1.398(5)
O6–Cl1	1.349(8)
O7–Cl2	1.397(6)
O8–Cl2	1.437(1)
O9–Cl2	1.352(1)
O10–Cl2	1.383(1)
O8A–Cl2	1.32(3)
O9A–Cl2	1.32(2)
O10A–Cl2	1.475(2)

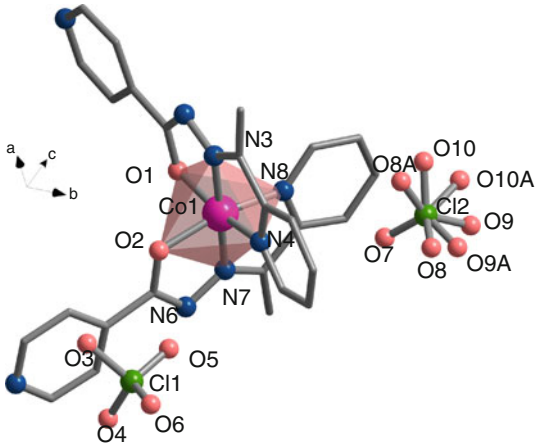

Fig. 2 Crystal structure of $[CoL_2](ClO_4)_2$

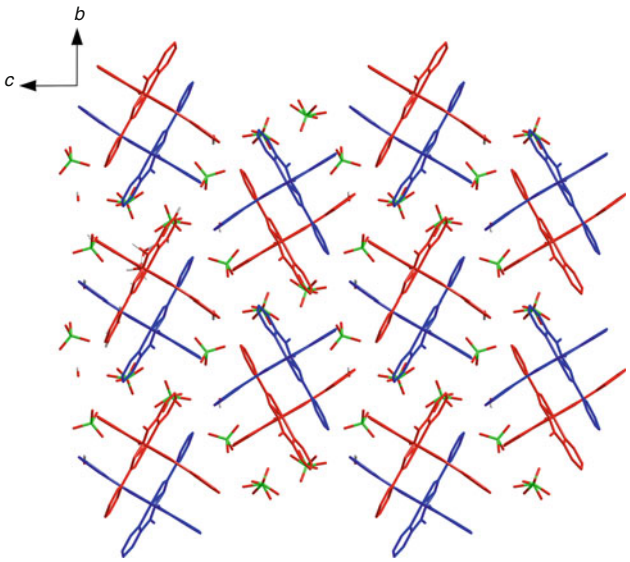

Fig. 3 Molecular packing of $[CoL_2](ClO_4)_2$ complex

azomethine. For the complexes the band group corresponding to amide I appear shifted by 5–54 cm^{-1} toward lower frequencies, which indicates the involvement of carbonyl group in coordination [24]. Also, a shift towards lower values of $\Delta\nu = 17–51$ cm^{-1} is observed for the frequencies characteristic to azomethine group of metal complexes with 2-acetyl-pyridyl-isonicotinoylhydrazone. This suggests the involvement of azomethine nitrogen in coordination with metallic ions [24].

In the IR spectra of the ligand, three mid intensity bands appear at 1581, 991 and 753 cm^{-1}, which are assigned to vibration frequency ν(Py ring), Py ring bending and γ (Py ring outside the plan), respectively.

In complexes **I–V**, **VII** and **VIII**, vibration frequency due to the Py ring is displaced to lower values. On the other hand,

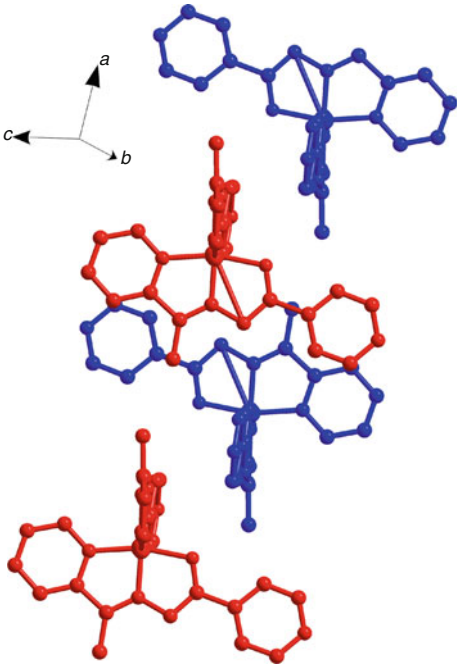

Fig. 4 π–π type interactions stacking of $[CoL_2](ClO_4)_2$ complex

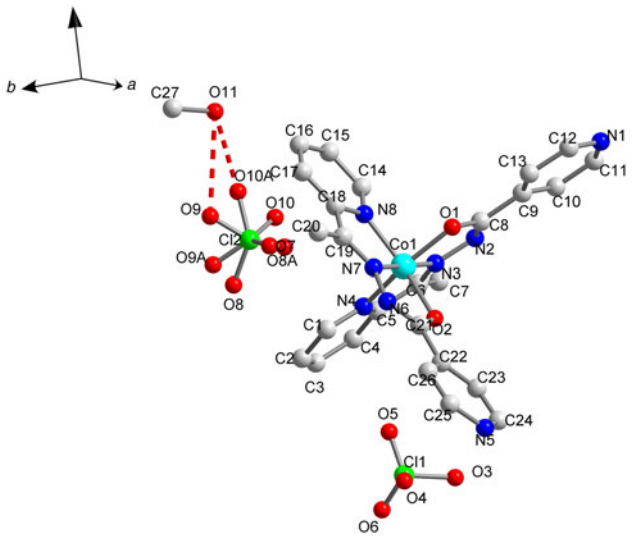

Fig. 5 Hydrogen bonds in $[CoL_2](ClO_4)_2$ complex

in the IR spectra of complexes the band corresponding the Py ring bending, which in ligand is at 991 cm^{-1}, is shifted to higher values, by $\Delta\nu = 19–79$ cm^{-1}. Displacements to higher values with $\Delta\gamma = 3–29$ cm^{-1} also appear for the typical band of γ (Py ring outside the plan). This information leads to the idea that pyridine nitrogen of 2-acetyl pyridine is involved in the coordination with metal ions [25, 26]. All data support the idea that in the **I–V**, **VII** and **VIII** complexes, the ligand works as tridentate NNO, being coordinated through the azomethine nitrogen, the pyridine nitrogen and carbonylic oxygen.

Table 4 Selected infrared absorption frequencies (cm^{-1}) of L and its complexes

Compounds	ν(OH)	ν(N–H)	ν(C=O) amide I	ν(C=N) azomethine	ν(Py ring)	Py ring bending	γ (Py ring outside the plan)
L	–	3190	1670	1623	1581	991	753
		3076					
$[CuL_2](ClO_4)_2$ (I)	3444	3075	1616	1572	1503	1056	770
$[CoL_2](ClO_4)_2$ (II)	3438	3096	1639	1606	1536	1020	782
$[NiL_2](ClO_4)_2$ (III)	3434	3075	1635	1599	1535	1010	755
$[MnL_2](ClO_4)_2$ (IV)		3077	1666	1601	1553	1012	775
$[ZnL_2](ClO_4)_2$ (V)	3421	3077	1634	1595	1542	1045	758
$[CuL_2(H_2O)_2](SO_4)\cdot 2.5H_2O$ (VI)	3446	3185	1647	1585	1539	982	715
$[CoL_2](SO_4)\cdot H_2O$ (VII)	3392	3178	1654	1596	1548	1058	755
$[NiL_2](SO_4)\cdot 3H_2O$ (VIII)	3400	3214	1659	1603	1551	1070	756
$[MnL_2(H_2O)_2](SO_4)\cdot 1.5H_2O$ (IX)	3566	3281	1662	1602	1546	984	701
		3094					
$[ZnL_2(H_2O)_2](SO_4)\cdot 3H_2O$ (X)	3474	3104	1664	1605	1548	983	707

In the IR spectra of complexes **VI**, **IX** and **X**, the band corresponding the Py ring bending and typical band of γ (Py ring outside the plan), are shifted to lower values, these indicating that pyridine nitrogen of 2-acetyl pyridine is not involved in the coordination with metal ions. In these complexes, the ligand works as bidentate NO, being coordinated through the azomethine nitrogen, and carbonylic oxygen.

The complexes **I**–**V** have in IR spectrum a very intense band in the domain of 1096–1117 cm^{-1} (ν_3) and a medium intense band at about 620 cm^{-1} (ν_4). This proves the existence of the ClO_4^- ion, and indicates that Td symmetry is not distorted [19].

The IR spectra of complexes **VI**–**X** also show the band attributed to the counteranion SO_4^{2-} [24].

Magnetic moments, electronic and EPR spectra

The magnetic moments for all complexes were determined at room temperature, using the diamagnetic correction [27] (Eq. 1):

$$\chi_D = kM \times 10^{-6}\ cm^3\ mol^{-1} \quad (1)$$

where M is the molecular weight of the compound and k a factor varying between 0.4 and 0.5.

The Schiff base presents in UV spectra two bands at 34,482 and 31,847 cm^{-1}, assigned to $\pi \rightarrow \pi^*$ and $n \rightarrow \pi^*$ transitions.

The electronic spectra of Co(II) complexes presents three bands attributed to the d-d transitions $^4T_{1g} \rightarrow {}^4T_{2g}$, $^4T_{1g}(F) \rightarrow {}^4A_{2g}$ and $^4T_{1g} \rightarrow {}^4T_{1g}(P)$, respectively. These transitions and the values of the field parameters correspond to those characteristic for an octahedral geometry [28]. For these complexes, the magnetic moments experimentally determined are 4.33 BM, and 4.85 MB indicating a high-spin character and excluding the oxidation to Co(III). These values are within the range 4.3–5.7 BM, corresponding to an octahedral geometry for cobalt ion [9].

The electronic spectra of Ni(II) complexes presents three bands, attributed to the $^3A_{2g} \rightarrow {}^3T_{2g}$, $^3A_{2g} \rightarrow {}^3T_{1g}$, and respectively, $^3A_{2g} \rightarrow {}^3T_{1g}$ (P) transitions, proper to an octahedral geometry for the nickel ion. For the Ni(II) complexes, the values of the magnetic moments are 3.20 BM and 3.47 MB. These are within the range 2.8–3.5 BM found for the paramagnetic Ni(II) complexes with an octahedral geometry [9].

The ligand field splitting energy ($10\Delta q$), interelectronic repulsion parameter (B) and nephelauxetic ratio (β) for the Co(II) and Ni(II) complexes were calculated using the secular equations given by König [29] and the values are presented in Table 5.

The Mn complexes present a signal in UV domain, assigned to a transfer of electric charge, according to the theory data for a d^5 ion. It is well known that the d–d transitions occur in the d^5 systems but those transitions are of very low intensities and hence we did not observe any d–d bands for such transitions [30]. The magnetic moments determined for the Mn(II) complexes are 6.01 BM and 5.65 MB. These values fall in the range 5.65–6.10 BM, and are appropriate to the manganese ion, with an octahedral environment [30].

In the spectra of Zn(II) complexes, the bands of the ligand appear shifted to lower values. For d^{10} ions, the UV spectrum does not indicate data about the environment. However, according to IR spectra, it was supposed that in

Table 5 Electronic spectral data and geometries for the ligand and its complexes

Compounds	Frequencies/cm^{-1}	Assignments	10Δq	*B*	*β*	Environment
L	34,482	$\pi \rightarrow \pi^*$	–	–	–	–
	31,847	$n \rightarrow \pi^*$				
$[CuL_2](ClO_4)_2$ (I)	33,898	$\pi \rightarrow \pi^*$	–	–	–	Octahedral
	26,041	$n \rightarrow \pi^*$				
	15,105	$z^2 \rightarrow x^2 - y^2$				
$[CoL_2](ClO_4)_2$ (II)	37,878	$\pi \rightarrow \pi^*$	7576	774,533	0,797	Octahedral
	30,303	$n \rightarrow \pi^*$				
	22,222	$^4T_{1g} \rightarrow {}^4T_{1g}(P)$				
	16,666	$^4T_{1g}(F) \rightarrow {}^4A_{2g}$				
	9090	$^4T_{1g} \rightarrow {}^4T_{2g}$				
$[NiL_2](ClO_4)_2$ (III)	25,773	$^3A_{2g} \rightarrow {}^3T_{1g}(P)$	8333	823,2	0,799	Octahedral
	11,574	$^3A_{2g} \rightarrow {}^3T_{1g}$				
	8333	$^3A_{2g} \rightarrow {}^3T_{2g}$				
$[MnL_2](ClO_4)_2$ (IV)	34,246	$\pi \rightarrow \pi^*$	–	–	–	Octahedral
	30,487	$n \rightarrow \pi^*$				
	27,472	CT				
$[ZnL_2](ClO_4)_2$ (V)	33,859	$\pi \rightarrow \pi^*$	–	–	–	Octahedral
	31,250	$n \rightarrow \pi$				
$[CuL_2(H_2O)_2](SO_4)\cdot 2.5H_2O$ (VI)	35,211	$n \rightarrow \pi^*$	–	–	–	Octahedral
	26,041	$n \rightarrow \pi^*$				
	12,690	$^2E_g \rightarrow {}^2T_{2g}$				
$[CoL_2](SO_4)\cdot H_2O$ (VII)	35,211	$\pi \rightarrow \pi^*$		624.6	0.643	Octahedral
	29,940	$n \rightarrow \pi^*$				
	25,641	$^4T_{1g} \rightarrow {}^4T_{1g}(P)$				
	18,939	$^4T_{1g}(F) \rightarrow {}^4A_{2g}$				
	11,737	$^4T_{1g} \rightarrow {}^4T_{2g}$				
$[NiL_2](SO_4)\cdot 3H_2O$ (VIII)	34,482	$\pi \rightarrow \pi^*$		934.53	0.907	Octahedral
	29,411	$n \rightarrow \pi^*$				
	27,739	$^3A_{2g} \rightarrow {}^3T_{1g}$				
	16,339	$^3A_{2g} \rightarrow {}^3T_{1g}$				
	10,020	$^3A_{2g} \rightarrow {}^3T_{2g}$ (P)				
$[MnL_2(H_2O)_2](SO_4)\cdot 1.5H_2O$ (IX)	34,246	$\pi \rightarrow \pi^*$	–	–	–	Octahedral
	30,674	$n \rightarrow \pi^*$				
	14,662	CT				
$[ZnL_2(H_2O)_2](SO_4)\cdot 3H_2O$ (X)	34,246	$\pi \rightarrow \pi^*$	–	–	–	
	26,881	$n \rightarrow \pi^*$				

Table 6 EPR data of the Cu(II) complex (I)

Compound	*g*		*H*/mT	
	$g_{\|}$	$g_{\perp}$	$H_{\|}$	$H_{\perp}$
$[CuL_2](ClO_4)_2$	2.2257	2.0627	303.091	327.033

this complex, the metallic ion is within an octahedral environment. The two complexes of Zn(II) are diamagnetic, as expected for the configuration of d^{10} [31].

The electronic spectra of the Cu(II) complexes, exhibit a large band at 15,105 and 12,690 cm^{-1}, respectively, which can be attributed to the $z^2 \rightarrow x^2 - y^2$ transition. This values together with the magnetic moment at 1.72 and 1.86 BM suggest an octahedral geometry for the Cu(II) ions [28].

The Cu(II) complex (I) was also examined by EPR spectroscopy and the values for $g_{\|}$ and $g_{\perp}$ were determined for the proper magnetic field (Table 6). The EPR spectra (Fig. 6) and the values of the magnetic field parameters require an elongated octahedral symmetry for the Cu(II) complex ($g_{\|} > g_{\perp}$).

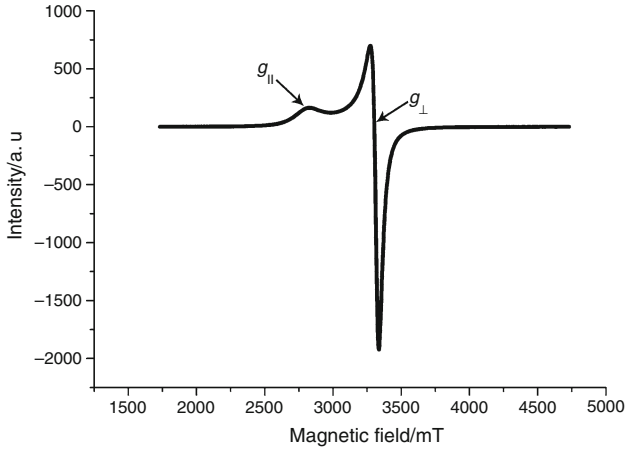

Fig. 6 EPR spectrum of $[CuL_2](ClO_4)_2$ complex at room temperature

Thermal analysis

Thermal analysis has proved to be useful in determining the crystal water content in complexes and their thermal stability and decomposition mode under a controlled heating rate. Due to the explosive nature of perchlorate complexes, the thermal properties of the sulphate complexes only have been investigated [32, 33].

The TG/DTA curve of the Schiff base (Fig. 7) showed a melting peak process located at 438 K (peak temperature on DTA curve). The melting process is followed by total decomposition. The remaining mass was 6.25%.

The determined temperature ranges and the corresponding percent mass losses of the complexes are given in Table 7.

The TG/DTA curves of $[CuL_2(H_2O)_2](SO_4)\cdot 2.5H_2O$ complex are represented in Fig. 8. The decomposition of Cu(II) complex follows three stages. The TG/DTA curve of

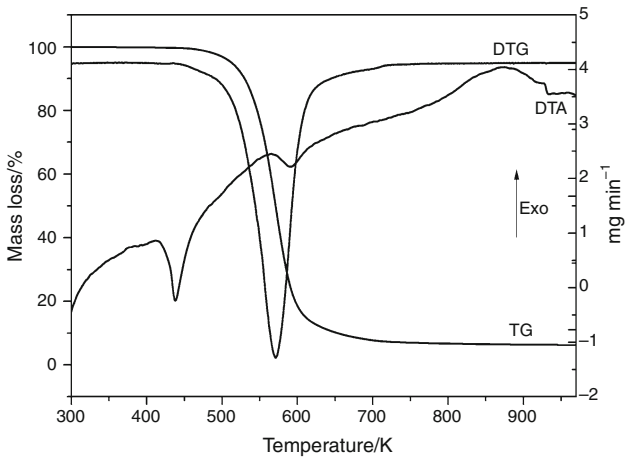

Fig. 7 TG/DTA curve of the ligand

$[CuL_2(H_2O)_2]$ $(SO_4)\cdot 2.5H_2O$ complex shows a mass loss between 303 and 378 K, with DTA peak at 370 K, due to the dehydration with a loss of two and a half lattice water molecules (exp. 7.61%, calc. 7.04%). The second stage between 378 and 430 K with DTA peak at 415 K corresponds to the removal of two coordinated water molecules. The third stage which occurs in the temperature range 430–1473 K, with two exothermal peaks at 526 and 1043 K, respectively, in the DTA curve, is corresponding to the removal of the ligand. The overall mass loss is observed to be 63.11%. The final residue, estimated as $CuSO_4$, has the observed mass 24.0%.

The DSC curve of $[CoL_2](SO_4)\cdot H_2O$ is shown in Fig. 9. The thermal decomposition of Co(II) complex occurs in two stages. The thermal dehydration of this complex takes place between 303 and 443 K, with a mass loss of 2.44% (calc. 2.83%). One mole of lattice water molecule is removed in this stage of dehydration. The process is accompanied by endothermal effect at 344 K in DTG curve. The second stage (from 443 to 1273 K) is due to the decomposition of ligand with observed mass loss of 74.09% (calc. 73.52%). This step is accompanied by a complex decomposition process with three consecutive peaks in DTA curve. The final residue, estimated as $CoSO_4$, has the observed mass of 23.47%, as compared to calculated value of 23.88%.

The TG/DTA curves of $[NiL_2](SO_4)\cdot 3H_2O$ complex are represented in Fig. 10.

The $[NiL_2](SO_4)\cdot 3H_2O$ complex shows almost the same two stage decomposition process as Co(II) complex. The first stage occurs in the temperature range 303–368 K, with the mass loss of 8.70% is due to the removal of three lattice water molecules (calc. 8.51%), corresponding to an endothermal peak at 353 K on DTA curve. The second step between 368 and 1473 K corresponds to the thermal decomposition with three exothermal peaks in the DTA curve. The process is complex and it is due to the total decomposition of the ligand. The observed mass loss in this temperature range is 65.20%. The residues are $NiSO_4$ with the observed mass of 26.12%.

The thermal decomposition of $[MnL_2(H_2O)_2](SO_4)\cdot 1.5H_2O$ follows three stages. The TG/DTA curve is given in Fig. 11.

The first step of thermal decomposition occurs in the range 403–394 K, corresponding to the removal of one and a half lattice water molecules (exp. 4.10%; calc. 4.287%). The second step (from 394 to 428 K) is due to the removal of two coordinated water molecules. The observed mass loss in this temperature range is 5.93% (calc. (5.70%). The third stage between 428 and 1260 K corresponds to the total decomposition of ligand. On DTA curve, the decomposition process is complex with at least three endothermal peaks. The final product estimated as $MnSO_4$,

Table 7 Thermoanalytical results for the complexes

Compounds	TG range/K	Mass loss found (calc.)/%	Assignments
$[CuL_2(H_2O)_2](SO_4)\cdot 2.5H_2O$ (VI)	303–378	7.61 (7.04)	Loss of 2.5 lattice water molecules
	378–430	5.28 (5.63)	Loss of two coordinated water molecule
	430–1473	63.11 (71.06)	Removal of the ligand part
	>1473	24.0 (25.0)	$CuSO_4$
$[CoL_2](SO_4)\cdot H_2O$ (VII)	303–443	2.44 (2.83)	Loss of one lattice water molecule
	443–1273	74.09 (73.52)	Removal of the ligand
	>1273	23.47 (23.88)	$CoSO_4$
$[NiL_2](SO_4)\cdot 3H_2O$ (VIII)	303–368	8.70 (8.51)	Loss of three lattice water molecules
	368–1473	65.20 (69.70)	Removal of the ligand
	>1473	16.12 (24.37)	$NiSO_4$
$[MnL_2(H_2O)_2](SO_4)\cdot 1.5H_2O$ (IX)	303–394	4.10 (4.28)	Loss of 1.5 lattice water molecules
	394–428	5.93 (5.70)	Loss of two coordinated water molecule
	428–1260	69.12 (69.18)	Removal of the ligand
	>1260	20.85 (21.75)	$MnSO_4$
$[ZnL_2(H_2O)_2](SO_4)\cdot 3H_2O$ (X)	303–416	8.64 (8.42)	Loss of three lattice water molecules
	416–443	5.13 (5.62)	Loss of two coordinated water molecule
	443–623	9.76 (10.93)	Removal of one molecule of SO_3
	623–1373	64.74 (65.64)	Removal of the ligand
	>1373	11.73 (11.07)	ZnO

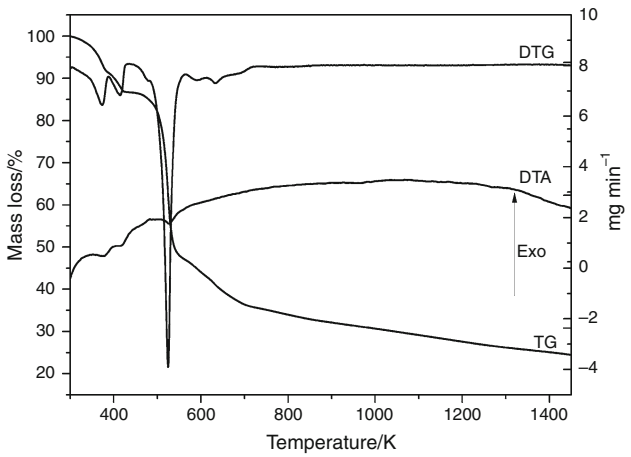

Fig. 8 TG/DTA curves of $[CuL_2(H_2O)_2](SO_4)\cdot 2.5H_2O$ complex

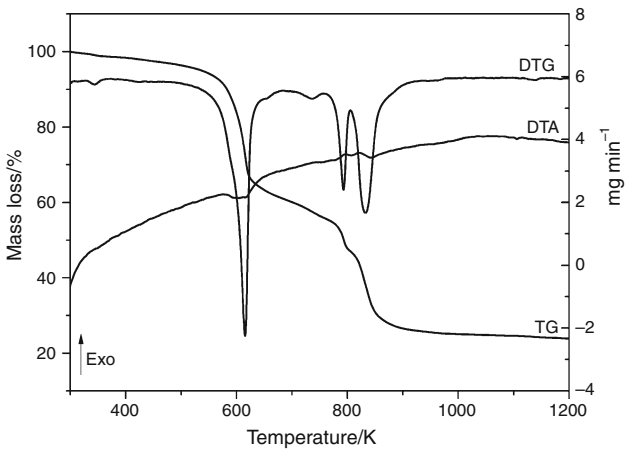

Fig. 9 TG/DTA curves of $[CoL_2](SO_4)\cdot H_2O$ complex

has the observed mass of 20.85%, compared with the calculated value of 21.75%.

According to TG/DTA analysis (Fig. 12), the thermal decomposition of $[ZnL_2(H_2O)_2](SO_4)\cdot 3H_2O$ complex undergo in four stages.

The first mass loss that occurs between 303 and 416 K, with the endothermal peak in the DTA curve at 397 K, corresponding to the removal of three lattice water molecules (exp. 8.64%; calc. 8.43%). The second step between 416 and 443 K corresponds to the loss of two coordinated water molecules (exp. 5.13%; calc. 5.62%). The third stage between 443 and 623 K corresponds to the loss of the SO_3 group. The observed mass loss is 9.76%, which is consistent with the theoretical value of 10.93%. The decomposition of the ligand was followed in the fourth stage between 623 and 1373 K, with a mass loss of 64.74% (calc. 65.64%). The end product, estimated as ZnO, has the observed mass of 11.73%, compared with the calculated value of 11.07%.

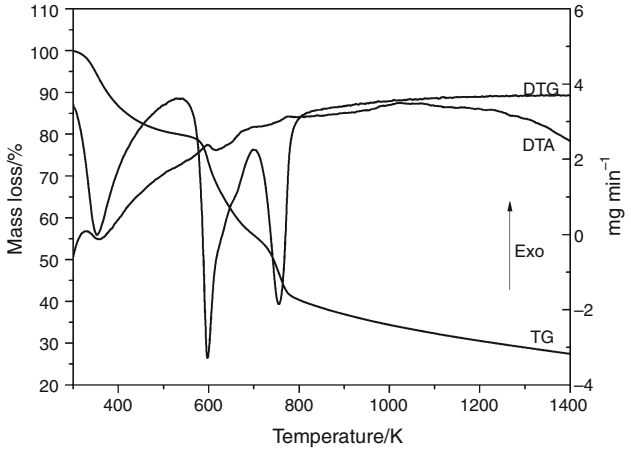

Fig. 10 TG/DTA curves of $[NiL_2](SO_4)\cdot 3H_2O$ complex

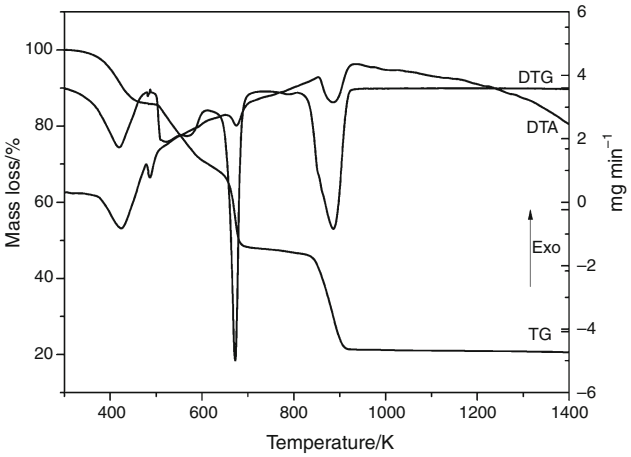

Fig. 11 TG/DTA curves of $[MnL_2(H_2O)_2](SO_4)\cdot 1.5H_2O$ complex

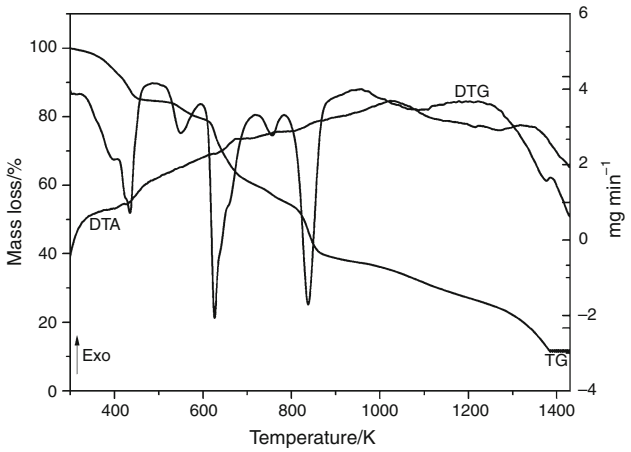

Fig. 12 TG/DTA curves of $[ZnL_2(H_2O)_2](SO_4)\cdot 3H_2O$ complex

Table 8 Preliminary test results to determine the antibacterial action of 2-acetyl-pyridyl isonicotinoylhydrazone complexes

Compounds	Zone diameter of inhibition Ø/mm		
	Staphylococcus aureus	*Escherichia coli*	*Salmonella Typhimurium*
L	10	6	12
$[CuL_2](ClO_4)_2$ (I)	4	4	6
$[CoL_2](ClO_4)_2$ (II)	12	7	12
$[NiL_2](ClO_4)_2$ (III)	7	4	4
$[MnL_2](ClO_4)_2$ (IV)	8	6	7
$[ZnL_2](ClO_4)_2$ (V)	4	4	4
$[CuL_2(H_2O)_2](SO_4)\cdot 2.5H_2O$ (VI)	11	6	8
$[CoL_2](SO4)\cdot H_2O$ (VII)	4	6	9
$[NiL_2](SO_4)\cdot 3H_2O$ (VIII)	10	7	8
$[MnL_2(H_2O)_2](SO_4)\cdot 1.5H_2O$ (IX)	12	4	8
$[ZnL_2(H_2O)_2](SO_4)\cdot 3H_2O$ (X)	7	4	4
References	*Staphylococcus aureus*	*Escherichia coli*	*Salmonella Typhimurium*
Ciprofloxacin	–	–	39
Gentamicin	–	1	–
Ampicilin	27	–	–

Antibacterial screening

The results of antibacterial screening of L and its complexes against *Staphylococcus aureus, Escherichia coli* and *Salmonella Typhimurium* are shown in Table 8.

All complexes have antibacterial activity of microbial species tested, with diameter of inhibition ranging between 4 and 12 mm. The complex **V** has the lowest antibacterial activity with a diameter of inhibition of 4 mm for all strains tested. It is noted that the most intensive

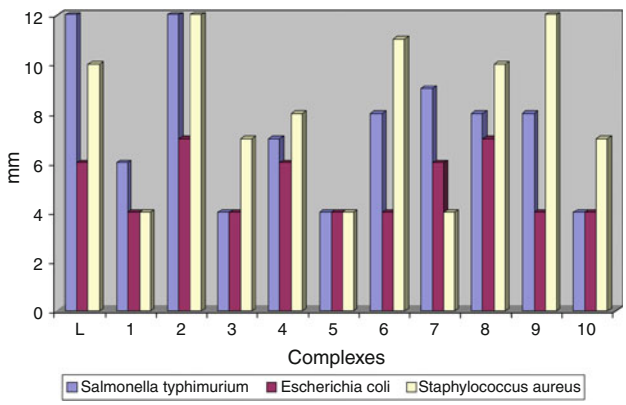

Fig. 13 The antimicrobial activity of ligand and its complexes

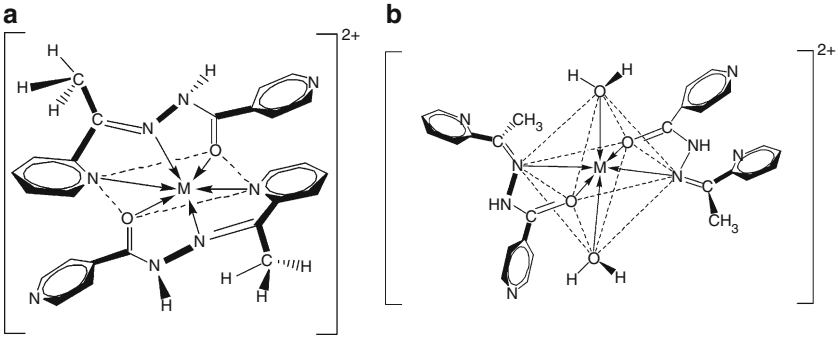

Fig. 14 Suggested structural formula of the complexes **a** I–V, VII and VIII. **b** VI, IX and X

antibacterial activity presents the complex 2 with a diameter of inhibition between 7 and 12 mm on all strains tested, which was more active on gram-positive cocci (Ø = 12 mm) (Fig. 13). A possible explanation [34] for the increased activity upon chelation is that in the chelated complex, the positive charge of the metal ion is partially shared with the donor atoms of the ligand, and a π-electron delocalization occurs over the whole chelate ring, thus increasing the lipophilic character of the metal chelate and favouring its permeation through the lipoid layers of the bacterial membranes and blocking the metal binding sites in the enzymes or microorganism.

Based on the above analytical, spectral and magnetic data together with the thermal decomposition studies, the new obtained complexes have the following proposed structural formula and the stoichiometry presented in Fig. 14a, b.

Conclusions

Ten new complexes of 2-acetyl-pyridyl-isonicotinoylhydrazone with Cu(II), Co(II), Ni(II), Mn(II) and Zn(II) perchlorate and sulphate were synthesized and characterized. All compounds were characterized by elemental analysis, IR and UV–Vis spectroscopy and magnetic measurements. The structural determination of Co(II) perchlorate complex was accomplished by X-ray diffraction. The spectral studies indicate that the ligand is N, N, O tridentate in seven complexes, and N, O bidentate in three complexes. The metal ions are six-coordinated, the coordination environment being slightly distorted octahedral. The thermal data are in agreement with the spectral and elemental data. Biological activity study shows that complexes exhibit a moderate activity against gram-negative and gram-positive bacteria.

Supplementary material

Crystallographic data for the structure in this article have been deposited with the Cambridge Crystallographic Data Centre, CCDC numbers: CCDC 809702. This data can be obtained free of charge at http://www.ccdc.cam.ac.uk/deposit (or from the Cambridge Crystallographic Data Centre, 12, Union Road, CAMBRIDGE, CB2 1EZ, UK; Tel: (44) 01223 762910; Fax: (44) 01223 336033; Email: deposit@ccdc.cam.ac.uk).

References

1. Chohan ZH, Sheazi SKA. Synthesis and characterization of some Co(II), Cu(II) and Ni(II) complexes with nicolinylhydrazine derivatives and their biological role of metals and anions (SO_4^{2-}, NO_3^-, $C_2O_4^{2-}$ and $CH_3CO_2^-$) on the antibacterial properties. Synth React Inorg Met-Org Chem. 1999;29:105–18.
2. Jayabalakrishnan C, Natarajan K. Synthesis, characterization and biological activities of ruthenium(II) carhonyl complexes containing bifunctional tridentate Schiff bases. Synth React Inorg Met-Org Chem. 2001;31:983–95.
3. Jeeworth T, Wah HLK, Bhowon MG, Ghoorhoo D, Babooram K. Synthesis and antibacterial/catalytic properties of schiff bases and Schiff base metal complexes derived from 2,3-diaminopyridine. Synth React Inorg Met-Org Chem. 2000;30:1023–38.
4. Savanini L, Chiasserini L, Gaeta A, Pellerano C. Synthesis and anti-tubercular evaluation of 4-quinolylhydrazones. Biorg Med Chem. 2002;10:2193–8.
5. Ochiai E-I. Bioinorganic chemistry. Boston: Allyn and Bacon; 1977.
6. Jaysukhlal R, Merchant D, Chothia S. Antituberculous Schiff bases. J Med Chem. 1970;13(2):335–6.
7. Biradar NS, Havinale BR. Dimeric square planar complexes of Cu(II) with aroyl hydrazones. Inorg Chim Acta. 1976;17:157–60.
8. Kakimoto S, Yashamoto K. Studies on antitubercular compounds. X. Condensation products of aldehydes and acid hydrazides of pyridine group. Pharm Bull. 1956;4(1):4–6.
9. Agarwal RK, Sharma D, Shing L, Agarwal H. Synthesis, biological, spectral and thermal investigations of cobalt(II) and nickel(II) complexes of N-isonicotinamido-2,4-dichlorobenzalaldimine. Bioinorg Chem Appl. 2006. doi:10.1155/BCA/2006/29234.
10. Gourbatsis S, Hadjiliadis N, Kalkanis G. The coordination chemistry of N,N′-ethylene bis(2-acetylpyridine imine) and N,N′-ethylene bis(2-benzoylpyridine imine); two potentially tetradentate ligands containing four nitrogen atoms. Trans Met Chem. 1990;15:300–8.
11. Stelzig L, Kotte S, Krebs B. Molybdenum complexes with tridentate NS_2 ligands. Synthesis, crystal structures and spectroscopic properties. J Chem Soc Dalton Trans. 1998;2921–26.
12. Rana A, Dinda R, Sengupta P, Ghosh S, Falvello LR. Synthesis, characterization and crystal structure of cis-dioxomolybdenum

(VI) complexes of some potentially pentadentate but functionally tridentate (ONS) donor ligands. Polyhedron. 2002;21:1023–30.
13. Tandom SS, Chander S, Thompson LK. Liganting properties of tridentate Schiff base ligands, 2[[(2-pyridinylmethyl)imino] methyl]phenol (HSALIMP) and 2-[[[2-(2-pyridinyl)ethyl]imino] methyl]phenol (HSALIEP) with Zn(II), Cd(II), Ni(II) and Mn(III) ions. X-ray crystal structures of the $[Zn(SALIEP)(NO_3)]_2$ dimer, $[Mn(SALIEP)_2](ClO_4)$ and $[Zn(AMP)_2(NO_3)_2]$. Inorg Chim Acta. 2000;300:683–92.
14. Oshio H, Toriumi MY, Takashima Y. Temperature-dependent crystallographic studies on ferric spin-crossover complexes with different spin-interconversion rates. Inorg Chem. 1991;30: 4252–60.
15. Nazir H, Yildiz M, Yilmaz H, Tahir MN, Ulku D. Intramolecular hydrogen bonding and tautomerism in Schiff bases. Structure of N-(2-pyridil)-2-oxo-naphthylidenemethylamine. J Mol Struct. 2000;524:241–50.
16. Jeffery JC, Thornton P, Ward MD. An unusual chainlike tetranuclear manganese(II) complex displaying ferromagnetic exchange. Inorg Chem. 1994;33:3612–5.
17. Ababei LV, Kriza A, Musuc AM, Andronescu C, Rogozea EA. Thermal behavior and spectroscopic studies of complexes of some divalent transitional metals with 2-benzoil-pyridilizonicotinoylhydrazone. J Therm Anal Calorim. 2010;101: 987–96.
18. Tătucu M, Kriza A, Maxim C, Stănică N. Synthesis and structural studies of Co(II), Ni(II) and Cd(II) complexes with 2-acetylpyridine. J Coord Chem. 2009;62(7):1067–75.
19. Kriza A, Tătucu M, Maxim C, Rău I. Metal(II) nitrate complexes with phenyl-2-pyridil-ketone: synthesis, characterization and antibacterial activity. Synth React Inorg Met-Org Chem. 2009;39: 419–24.
20. Stoe&Cie. X-AREA (version1.18). Darmstadt, Germany: Stoe&Cie; 2002.
21. Sheldrick GM. SHELXS-97, a program for the solution of crystal structures. Germany: University of Gottingen; 1997.
22. Pelczar MJ, Chan ECS, Krieg NR. Microbiology. 5th ed. New York: Blackwell Science; 1998. p. 535.
23. Geary WJ. The use of conductivity measurements in organic solvents for the characterization of coordination compounds. Coord Chem Rev. 1971;7:81–122.
24. Nakamoto K. Infrared spectra of inorganic and coordination compounds. 2nd ed. New York: Wiley-Interscience; 1970.
25. Serna EZ, Urtiaga KM, Barandika MG, Cortes R, Martin S, Lezama L, Arriotua MI, Rojo T. Dicubane-like tetrameric cobalt(II)-pseudohalide ferromagnetic clusters. Inorg Chem. 2001;40:4550–5.
26. Serna EZ, Urtiaga KM, Barandika MG, Cortes R, Lezama L, Arriotua MI, Rojo T. Investigation of the CuII/NCS–/dpk reaction system in CH_3OH [dpk = Di(2-pyridyl) Ketone]: isolation, structural analysis and magnetic properties of a dimer and a 1D polymer with the same empirical formula $[Cu(NCS)_2(dpk{\cdot}CH_3OH)]$. Eur J Inorg Chem. 2001;2001:865–72.
27. Kahn O. Molecular magnetism. New York: VCH; 1993. p. 2.
28. Lever ABP. Inorganic electronic spectroscopy. Amsterdam, The Netherlands: Elsevier; 1984.
29. König E. The nephelauxetic effect calculation, accuracy of the interelectronic repulsion parameters I. Cubic high-spin d2, d3, d7 and d8 systems. Struct Bonding. 1971;9:175–212.
30. Aurkie R, Banerjee S, Sen S, Butcher RJ, Rosair GM, Garland MT, Mitra S. Two Zn(II) and one Mn(II) complexes using two different hydrazone ligands: spectroscopic studies and structural aspects. Struct Chem. 2008;19(2):209–17.
31. Selwood PW. Magnetochemistry. New York: Interscience Publisher, Inc.; 1956.
32. Wei C, Rogers WJ, Mannan MS. Detection of autocatalytic decomposition behavior of energetic materials using APTAC. J Therm Anal Calorim. 2006;83:125–30.
33. Sing G, Pande DK. Studies on energetic compounds. Part 40. Kinetics of thermal decomposition of some bis(propylenediamine)metal perchlorate complexes. J Therm Anal Calorim. 2005;82:353–60.
34. Chohan ZH, Kausar S. Synthesis, characterization and biological properties of tridentate NNO, NNS and NNN donor thiazole-derived furanyl, thiophenyl and pyrrolyl Schiff bases and their Co(II), Cu(II), Ni(II) and Zn(II) metal chelates. Met Based Drugs. 2000;7(1):17–22.